CBR-2016-2028-ver9-Panichelli_1P
Type: research-article

CANCER BIOTHERAPY AND RADIOPHARMACEUTICALS
Volume 31, Number 5, 2016

DOI: 10.1089/cbr.2016.2028

Original Article

AU1 ▶

Imaging of Brain Tumors with Copper-64 Chloride: Early Experience and Results

AU2 ▶

Paola Panichelli,[1] Carlo Villano,[2] Angelina Cistaro,[3] Andrea Bruno,[4] Francesco Barbato,[5] Arnoldo Piccardo,[6] and Adriano Duatti[7]

Abstract

Objectives: To conduct the first investigational study that is aimed at evaluating the ability of the simple salt $^{64}CuCl_2$ to diagnose cerebral tumors in patients affected by glioblastoma multiforme (GBM).
Methods: Nineteen patients with a documented history and radiologic evidence of brain tumors were enrolled in the study. Eighteen patients were diagnosed with GBM, and one patient was diagnosed with grade II astrocytoma. After initial cerebral magnetic resonance imaging (MRI), patients were administered with $^{64}CuCl_2$ (13 MBq/kg) and brain positron emission tomography (PET)/computed tomography (CT) imaging was performed at 1, 3, and 24 hours after administration. Standardized uptake values (SUVs) were calculated and used to figure out the pharmacokinetic profile of the tracer. Absorbed radiation doses were estimated using OLINDA/EXM.
Results: Copper-64 chloride clearly visualized brain cancerous lesions within 1 hour after injection, with stable retention of radioactivity at 3 and 24 hours. Excellent agreement was found between PET/CT and MRI. No uptake of the tracer was observed in low-grade astrocytoma. The agent cleared rapidly from the blood and was mostly excreted through the liver, without significant kidney washout. Analysis of time variation of SUV_{max} values showed persistent uptake in malignant tissues with a slight increase of radioactive concentration at 24 hours.
Conclusions: Copper-64 chloride has favorable biological properties for brain imaging and warrants further investigation as a diagnostic tracer for GBM.

Key words: brain tumors, copper-64, copper-64 chloride, glioblastoma multiforme, neuroimaging, PET imaging

Introduction

Glioblastoma multiforme (GBM) is the most common primary malignancy of the central nervous system (CNS), and it is associated with an exceptionally poor prognosis. GBMs are infiltrative tumors that usually spread through brain parenchyma, thus making surgical eradication extremely arduous.[1–5]

Neuroimaging plays an essential role in the diagnosis of human brain tumors. Conventional diagnostic methods mostly rely on computed tomography (CT) and magnetic resonance imaging (MRI). Anatomical imaging is most commonly carried out with MRI, which is the current standard diagnostic modality for brain tumors. However, although MRI with contrast is generally superior to CT for imaging brain tumors, CT is still the most widely employed imaging method to detect anatomical abnormalities that are linked to malignant growth.[6–9]

These diagnostic modalities provide mostly anatomical information. Complementary diagnostic methods that enable elucidation of the metabolic characteristics of tumor tissue are required to achieve a more fundamental molecular picture of the disease. Positron emission tomography (PET) is an intrinsically molecular imaging technology that may potentially

AU3 ▶

[1]Advanced Center of Oncology, ACOM, Macerata, Italy.
[2]Hospital ''Santo Spirito,'' Pescara, Italy.
[3]Positron Emission Tomography Centre, IRMET, Affidea, Turin, Italy.
[4]ASST ''Papa Giovanni XXIII,'' Bergamo, Italy.
[5]CMO Center, Naples, Italy.
[6]Ospedali Galliera, Genoa, Italy.
[7]Department of Chemical and Pharmaceutical Sciences, University of Ferrara, Ferrara, Italy.

AU4 ▶

Address correspondence to: Adriano Duatti, Department of Chemical and Pharmaceutical Sciences, University of Ferrara; Via L. Borsari, 46, 44121 Ferrara, Italy
E-mail: **dta@unife.it**

allow extraction of metabolic information by monitoring processes such as glucose metabolism, cellular proliferation, hypoxia, and amino-acid transport. A variety of diagnostic agents have been investigated for brain tumor imaging, including tracers targeting integrin expression and angiogenesis (e.g., ^{18}F-Galacto-RGD[10]), and for imaging of hypoxia (e.g., ^{18}F-fluromisonidazole[11]). Accumulation of the radiolabeled amino acids *O*-(2-^{18}F-fluoroethyl)-L-tyrosine (^{18}F-FET)[12] and ^{11}C-methionine[13] in cerebral tumors is, presumably, linked to increased expression of the L-type amino-acid transporters in cancer cells, whereas the radiolabeled thymidine analog 3′-deoxy-3′-^{1}8F-fluorothimidine (^{18}F-FLT)[12] is employed as a surrogate marker of proliferation, though its uptake mechanism has still to be clearly elucidated. Despite this potential, the incremental diagnostic value of PET imaging in assessing the pathophysiology of brain tumors has not yet been fully established.

Current interest in copper-based PET imaging is due to both increased availability of a number of copper radionuclides with different half-lives (^{60}Cu, 23.7 minutes; ^{61}Cu, 3.3 hours; ^{62}Cu, 9.76 minutes; ^{64}Cu, 12.7 hours; ^{67}Cu, 61.83 hours) and decay properties. In particular, the radioisotope ^{64}Cu is easily produced by bombardment of a highly enriched ^{64}Ni target using a conventional medical cyclotron. This radionuclide decays through the concomitant emission of β^+ (17.8%) and β^- (38.4%) particles, and Auger electrons (43.8%) and, thus, could be potentially used as a theranostic agent for both diagnosis and therapy.[14,15]

Copper plays an essential role in human physiology, as it is required for conducting key biological functions. Accordingly, the metabolism of copper is tightly regulated and involves various transporters and copper-binding proteins. Among those, the high-affinity copper transporter CTR1 is believed to mediate cellular copper uptake.[16,17] However, it was observed that copper metabolism is altered in cancer patients and elevated copper levels have been found in both serum and tumor tissue in a variety of cancers. In particular, many preclinical studies have demonstrated an effect of copper on cancer development. A comparison of malignant and normal human tissue samples demonstrated that copper concentration was ~50% higher in the neoplastic tissues. These studies support the hypothesis that elevated tissue copper levels may play a relevant role in the development of a malignant process by either stimulating cancer cell proliferation or acting as a limiting factor for tumor growth.[18–20] Although the molecular and cellular mechanisms by which copper levels modulate tumor progression still remain largely unclear, the crucial involvement of copper ions in cancer development reasonably prompts a consideration of the hypothesis that it may potentially be employed as a specific and selective tumor imaging agent for PET. Because of its unique biological role, the study of diagnostic copper radioisotopes may open new windows for the molecular imaging of cerebral tumors by exploiting alternative biomolecular pathways that are not accessible with other PET agents.

The present work reports results obtained from the first exploratory clinical study in patients affected by GBM, and administered intravenously by Cu-64 under the simple chemical form of dichloride salt. Thus, the aim of this study was to provide preliminary clinical evidence on the potential diagnostic role of Cu-64 ions for imaging malignancies in the CNS. Previous preclinical studies in animal models[21] have already convincingly supported this hypothesis, but definite evidence in humans has not yet been reported. Since, according to our search, there are no previous published data in humans on the use of $^{64}CuCl_2$ as an imaging agent for brain tumors, an important advantage of conducting a preliminary exploratory investigation with this new radiopharmaceutical is to confirm preclinical data, thus facilitating translation of results into clinical applications.

Methods

Study Design

The institutional review boards of the participating medical institutions approved all procedures described in the following study. Patients diagnosed with GBM were invited to participate, screened for eligibility, and provided written informed consent. MRI was employed as a reference standard imaging modality for visualizing brain tumors. Characterization of the type of cerebral tumor was always confirmed by histological analysis of biopsied tissue samples. After undergoing baseline examinations as an additional investigation to routine care, patients were subjected to a first accurate brain MRI study with contrast medium not later than 2 weeks before the PET/CT scan to define the morphological parameters and characterization of the lesion. Then, patients received the study radiopharmaceutical and were followed for 24 hours to collect brain PET/CT tomographic images followed by a final MRI brain scan as a control. In particular, PET/CT scans were performed at 1, 3, and 24 hours postinjection (p.i.).

To evaluate potential hepatic radiotoxicity of $^{64}CuCl_2$ administration, blood tests were carried out on all patients by withdrawing 15 mL of a venous blood sample and by determining the following parameters: complete blood count, hematocrit, hemoglobin, haptoglobin, C-reactive protein, aspartate transaminase (AST), alanine transaminase (ALT), alkaline phosphatase (ALP), albumin, total bilirubin, gamma-glutamyl transferase (gamma GT), lactate dehydrogenase (LDH), total proteins, serum creatinine, and azotemia. A blood test was carried out immediately before administration of the radiopharmaceutical, and then after whole-body scans at 3 and 24 hours p.i. A final blood test was performed 10 days after injection during the routine follow-up medical control. Electrocardiography was carried out during the first baseline examination, then at 24 hours p.i., and after 10 days during the final control.

Patient Characteristics

All patients (9 men and 10 women, age range 23–81 years) had a documented history and radiological evidence of cerebral lesions. Eighteen patients were diagnosed for cerebral GBM, and one patient was affected by grade II astrocytoma. Two patients had brain tumors associated with lung cancer, and for the other two patients brain lesions were linked to primary breast cancer. Summary of patients' characteristics and treatments received before inclusion in this study are listed in Table 1. ◀T1

Radiopharmaceutical preparation

Copper-64 dichloride (average specific activity, 3700 MBq/μg, radiochemical purity >99%, radionuclidic purity >99%)

Table 1. Summary of Patient Characteristics

Patient no.	Age	Sex	Weight (kg)	Year of initial diagnosis	Diagnosis[a]	Prior surgery	Prior therapy	PET/CT MRI[b]
001	70	M	74	2011	GBM	Yes	RT + CHT	Yes
002	68	F	61	2012	GBM	None	RT	Yes
003	73	F	58	2015	GBM associated with primary breast cancer	Yes	Hormone therapy (antiestrogenic)	Yes
004	69	M	73	2015	GBM	None	CHT	Yes
005	52	F	64	2015	GBM	Yes	None	Yes
006	44	F	58	2014	GBM	None	CHT + RT	Yes
007	54	F	66	2014	GBM	Yes	None	Yes
008	45	F	60	2013	Grade II astrocytoma	Yes	RT + CHT	No
009	72	F	66	2014	GBM	Yes	RT + CHT	Yes
010	73	F	54	2014	GBM	Yes	RT	Yes
011	80	M	67	2014	GBM	Yes	RT + CHT	Yes
012	23	M	79	2014	GBM	None	RT + CHT	Yes
013	44	M	80	2014	GBM	Yes	None	Yes
014	62	F	58	2014	GBM associated with primary breast cancer	Yes	CHT + RT	Yes
015	57	M	69	2012	GBM	Yes	CHT?	Yes
016	67	F	58	2014	GBM associated with metastatic primary lung tumor	None	CHT + RT	Yes
017	64	M	73	2013	GBM	Yes	None	Yes
018	61	M	81	2015	GBM	None	RT + CHT	Yes
019	55	M	76	2015	GBM associated with primary squamous cell carcinoma in the right pulmonary hilum	Yes	RT + CHT	Yes

All patients were injected with the same activity/body mass ratio of 13 MBq/kg. Acquisition times were 1, 3, and 24 hours postinjection.
[a]Diagnosis was confirmed by analysis of cerebral samples obtained by biopsy.
[b]Consistency between PET/CT and MRI diagnosis.
CHT, chemotherapy (temozolomide); CT, computed tomography; GBM, glioblastoma multiforme; MRI, magnetic resonance imaging; PET, positron emission tomography; RT, radiation therapy.

was produced by following a procedure previously reported.[22] Briefly, highly enriched ^{64}Ni was electroplated on a gold disk, and Cu-64 was then produced by bombardment of the resulting ^{64}Ni target with a proton current of 18 μA, at an energy of 14.6 MeV by using an 18-MeV cyclotron (IBA). After bombardment, ^{64}Cu was separated from the ^{64}Ni target and purified from other contaminants by chromatography and by using an ion-exchange column that was prepared with a slurry of AGl ×8 anion-exchange resin (Biorad Laboratories) that was filled into a glass column with dimensions 1.0 × 30 cm. Activity was eluted with concentrated HCl (1.0 M) and filtered through a 0.2-μm filter (Merck Millipore), yielding high-specific activity ^{64}Cu as anionic copper chloride complexes. Radionuclidic and radiochemical purities were assessed as previously described.[22] Briefly, these procedures were as follows. Radionuclidic purity and half-life of ^{64}Cu were measured by using an HPGe detector (Ortec). The peaks at 511.0 keV, 1022.0 keV, and 1345.8 keV identified ^{64}Cu. Acceptable limits of radionuclidic purity were set as follows: ^{64}Cu ≥99.5%, ^{61}Co ≤0.260%, ^{61}Cu ≤0.150%, ^{62}Cu ≤0.0.45%, ^{55}Co ≤0.015%, ^{58}Co ≤0.015%, and ^{60}Cu ≤0.010%. The presence of other nonradioactive metallic impurities was assessed by inductively coupled ionization mass spectrometry (ICP-MS 7500; Agilent Technologies), and their concentrations were always lower than 20 μg/Ci of ^{64}Cu.

Radiochemical purity (RCP) was determined by a reaction of $^{64}CuCl_2$ with the ligand TETA (1,4,8,11-tetraazacyclotetradecane-*N,N′,N″,N‴*-tetraacetic acid), which shows a high binding affinity for this metal.[23] A fixed quantity of TETA (0.01 μg) was reacted with aliquots of $^{64}CuCl_2$ (2960–3700 Bq) in ammonium acetate buffer (pH 5.5), at 35°C for 60 minutes, while keeping constant the total volume (120 μL). Thin-layer chromatography on silica-gel plates, developed using a 1:l mixture of methanol and ammonium acetate (10%), was employed to measure radioactivity associated with the complex $[^{64}Cu(TETA)]^{2-}$ as detected by radiochromatography ($R_f = 0.00$ corresponds to free ^{64}Cu, whereas $R_f = 0.42$ corresponds to the radiocompound). Since in these conditions complexation of ^{64}Cu by TETA is almost quantitative, RCP was considered a reliable measure of ^{64}Cu-specific activity. Only samples with RCP ≥99% were released. This fully validated method provides an easy procedure for routine measurement of RCP and specific activity of ^{64}Cu solutions.

Terminal sterilization of the final solution was carried out by autoclaving for 20 minutes at 121°C under a pressure of 100 kPa.

Image acquisition

The verification of the cross-calibration between the PET scanner and the dose calibrator was performed by a uniform phantom filled with a $^{64}CuCl_2$ solution of 50 Bq/mL. This phantom was scanned with a single-bed acquisition of 3 minutes. The image was reconstructed with the same parameters, and corrections were as employed for clinical image reconstruction.

After intravenous (i.v.) injection of $^{64}CuCl_2$ (13 MBq/kg), images of the brain region and whole-body PET/CT scans were acquired at 1, 3, and 24 hours p.i. The mean and standard deviation of the administered mass of $^{64}CuCl_2$ was 0.23 ± 0.002 μg (range, 0.28–0.19 μg). The mean administered activity was 872.3 ± 0.8 MBq (range, 1053–702 MBq). PET/CT data acquisition was performed by using a Biograph 6 HiRez TruePoint PET/CT scanner (Siemens Healthcare) with an axial field of view (FOV) of 700 mm and a trans-axial FOV of 605 mm. Axial resolution for full-width-at-half-maximum (FWHM) was 4.7 and 5.7 mm at 1 and 10 cm, respectively. Trans-axial resolutions for FWHMs were 4.2 and 4.8 mm, respectively. PET images were obtained in 3D mode, with an acquisition time of 10 minutes per bed position. PET data were reconstructed by using OSEM iterative reconstruction algorithm with the following parameters: six iterations and 21 subsets, matrix size of 128×128 pixels, zoom 2.5, and Gaussian postreconstruction filter (FWHM, 2.0 mm). This setup was applied for both whole-body and brain imaging. A low-dose CT scan was acquired before each of the subsequent PET scans, modulated by the Care Dose 4D automatic exposure control system, and used for attenuation correction. The following acquisition parameters were utilized: 140-kVp tube voltage, 80-mA Care Dose 4D reference current, spiral acquisition type, 0.8 pitch, 1.2-mm collimation, 3.75-mm slice thickness, 3.270-mm slice interval, 0.5-second rotation, 700-mm SFOV for transmission scan, 300-mm SFOV for registered image, and 512×512-pixels image matrix.

Brain MRI data acquisition was performed using a contrast medium (Gadovist; 0.1 mmol/kg) and a 1.5-T scanner (Gyroscan NT; Philips Healthcare) with a 30 mT/m maximum gradient capability. Imaging was performed using a brain coil and collecting multiparametric MRI (mMRI) by means of associating T1- and T2-weighted imaging (T1/T2WI) with functional sequences such as diffusion-weighted imaging and dynamic contrast-enhanced imaging (DCE-MRI). The conventional MR imaging study consisted of an axial T1-weighted sequence (TR 577/TE 10). The T1-weighted sequence was acquired at a section thickness of 4 mm, within a matrix of 240×320 pixels and an FOV of 210×210 mm. The T2-weighted sequence (TR 4370/TE 97) was acquired at a section thickness of 4 mm, with a matrix size of 240×320 pixels and an FOV of 230×230 mm. The DCE-MRI was acquired at a section thickness of 2.5 mm, with a matrix size of 216×288 pixels and an FOV of 240×320 mm.

Image analysis

Two blinded nuclear medicine specialists evaluated PET/CT images. To quantify $^{64}CuCl_2$ uptake, regions of interest (ROI) were drawn manually around the lesions to include areas where the uptake was ≥10% of the maximum activity found in that region. Volume of interest (VOI) was defined around each region as a series of ROIs on adjacent slices, and standardized uptake values (SUV_{max}) were calculated using the maximum concentration within the VOI (SUV is defined as the activity concentration in kBq/mL found in the ROI at a fixed time point divided by the decay-corrected amount of injected activity in kBq normalized to the patient's measured weight expressed in grams).[24] The differential in tracer accumulation between normal and tumor tissues within the ROI was evaluated by a comparison with ROIs/VOIs positioned along the same line opposite to the lesion where no uptake was observed.

Organ-absorbed radiation dose estimates

The organ-normalized cumulated activity from the nondecay-corrected time/activity curves (not shown here) of the selected organs was calculated (Table 3) and entered into OLINDA/EXM software, as developed by M. Stabin, R. Sparks, and E. Crowe, to estimate organ-absorbed doses (Table 4).[25] The adult male model was used for all patients. The complete radiation dose estimates for all subjects were used to generate the descriptive statistics. The radiation doses to salivary glands and tumors were determined using spherical S values as implemented in OLINDA/EXM.

Results

Imaging studies and tissue distribution

As explained earlier, ROIs were drawn manually for selected organs (brain, liver, kidneys, spleen, and vertebrae L4 and L5) for every PET/CT scan on the co-registered CT serial axis images for determination of the peak activity within the organ region and for calculation of SUV_{max}. In turn, SUV_{max} estimates have been used to obtain a simplified picture of uptake and retention of Cu-64 in brain tumors as well as of the whole-body tracer's biodistribution.

Whole-body PET images for patients administered with $^{64}CuCl_2$ (Fig. 2) revealed high liver uptake without significant kidney washout. Uptake was also observed in the renal cortex, bowel, salivary glands, and parotid glands. These findings are consistent with previous biodistribution data of $^{64}CuCl_2$ collected in normal subjects where the liver was found to be the major natural target organ for Cu-64, as expected from the well-established biological behavior of copper ions.[26] In patients involved in the present study, malignant tissues in the CNS could be clearly detected within 1 hour after injection. Average SUV values (SUV_{mean}), calculated inside the whole ROI, in all patients and at all time points, were 0.03 in normal brain tissue and 1.55 in tumor tissue, showing that ^{64}Cu ions were selectively accumulated in cancerous lesions. No detectable washout of radioactivity from cancer cells was observed over time as revealed by SUV_{max} values measured at 1, 3, and 24 hours p.i., and as summarized in Table 2. Conversely, a slight, but significant ◀T2 increase of SUV_{max} was measured at 3 and 24 hours after injection of the tracer, thus suggesting a small increase of radioactivity concentration in cancerous cells at later times.

A high uptake of $^{64}CuCl_2$ was observed in all patients diagnosed with cerebral tumor except in one patient affected by low-grade astrocytoma. A representative example is illustrated in Figure 1, which reports the MRI scan of a patient with ◀F1 GBM (patient 020) and the corresponding PET/CT image registered 1 hour after an intravenous injection of $^{94}CuCl_2$. This patient did not undergo previous surgical removal of the large tumor, but only received radiation therapy and chemotherapy (CHT). Images reveal an excellent matching between diagnostic results collected with the two imaging modalities.

CT and PET/CT images of patient 01 taken at 1, 3, and 24 hours after administration of $^{64}CuCl_2$ are reported in Figure 2. These images show the persistent retention of the ◀F2

Table 2. SUV_{max} Values Measured in Patients' Brain Lesions at Different Time Points

Patient no.	*1 hour*	*Time 3 hours*	*24 hours*
001	3.9	4.2	4.4
002	3.2	3.6	3.7
003	4.2	4.5	4.8
004	3.6	3.8	4.0
005	6.3	7.1	7.3
006	5.4	5.8	5.9
007	3.2	3.5	3.5
008	0.2	0.18	0.3
009	5.1	5.5	5.6
010	3.2	3.6	3.7
011	3.8	4.2	4.4
012	3.9	4.4	4.5
013	4.2	4.9	5.0
014	6.1	6.9	7.0
015	4.7	5.3	5.5
016	4.6	5.1	5.3
017	3.8	4.3	4.5
018	5.9	6.4	6.5
019	4.7	5.2	5.3

SUV, standardized uptake value.

activity in the cerebral lesions, which slightly increased over time (Table 2). The same figure reports whole-body PET scans of patient 05 at 1 and 24 hours p.i., showing the initial high liver uptake that partially vanished at later times.

Copper-64 chloride also efficiently visualized brain lesions in patients suffering from another primary cancer. In this study, two patients with breast cancer and two patients with lung cancer were administered with the tracer. Figure 3 displays the brain PET/CT of a patient affected by metastatic lung cancer. Results clearly revealed the presence of cerebral lesions.

One patient was diagnosed with low-grade astrocytoma confirmed by biopsy after surgical removal of the lesion (patient 008). Initial MRI and PET/CT images before surgery are reported in Figure 4. The observed value of SUV_{max} in this region was particularly low and comparable to that found in the opposite nontumor area used as a reference, thus revealing that no $^{64}CuCl_2$ uptake was observed in this nonmalignant tumor despite the anatomical lesion being clearly manifested in the corresponding MRI scan.

Dosimetry

Table 3 reports the organ-normalized cumulative activity (MBq hours/MBq), and Table 4 depicts the mean estimated absorbed radiation dose for organs (mSv/MBq). The liver was the organ with the highest normalized cumulative activity (6.9 MBq hours/MBq) and absorbed dose (0.321 mSv/MBq). Kidneys received a minimal dose due to the very low renal excretion of the tracer. Radioactivity concentration in the cerebral region was low and almost completely localized in the brain tumor as demonstrated by the high SUV_{max} values. Organ dosimetric data were in good agreement with previous estimates as measured in patients with prostate cancer administered with $^{64}CuCl_2$.[26]

Safety

Because of potential copper toxicity and significant dose received by some target organs, particularly the liver, patients were carefully evaluated and monitored during the study. A number of blood tests have been carried out on each patient immediately after administration of the tracer and at different times p.i., to detect any sign of metabolic alterations. Concomitantly, heart functionality was also checked by electrocardiography. These control tests were repeated during the patient's final control 10 days after the last scan. There were no adverse or clinically detectable pharmacological effects in any of the 19 subjects. No significant changes in vital signs or from results of laboratory studies and electrocardiograms were observed. According to these observations, it appeared that the administration of the tracer was well tolerated by all patients and, in particular, the liver function was not affected by the high accumulation of ^{64}Cu radioactivity determined by the normal biological uptake of copper ions in this organ.

Discussion

The current availability of a few copper radioisotopes having decay characteristics that are suitable for PET imaging has allowed visualization of the biodistribution of copper in intact living organisms. More specifically, the biological fate of copper(II) ions, when intravenously injected under the simple chemical form of chloride salt, can be easily monitored using its radioactive counterpart $^{64}CuCl_2$.[27–31] Because of its biological role, it was reasonable to expect that radioactive copper could trace fundamental biomolecular processes having high diagnostic relevance for some

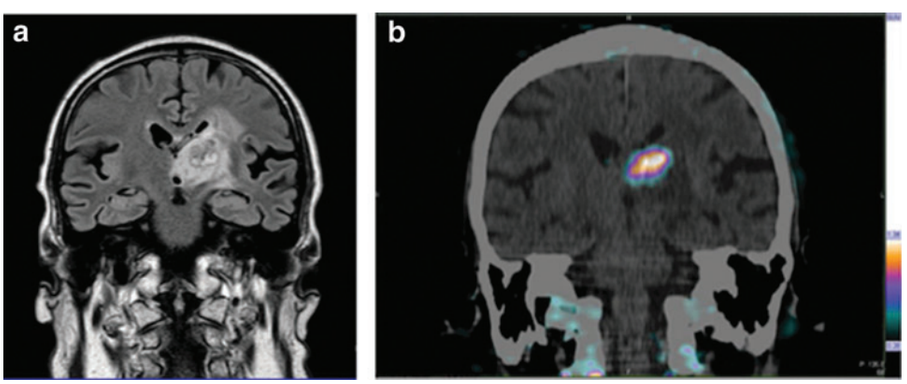

FIG. 1. Representative MRI **(a)** and PET/CT **(b)** brain images of a patient with GBM in the *left* thalamus (patient 018). Lesion size as measured by MRI was 31.22 mm. MRI scan was collected 1 week before injection of $^{64}CuCl_2$, whereas PET/CT was collected at 1 hour after administration of the tracer. CT, computed tomography; GBM, glioblastoma multiforme; MRI, magnetic resonance imaging; PET, positron emission tomography.

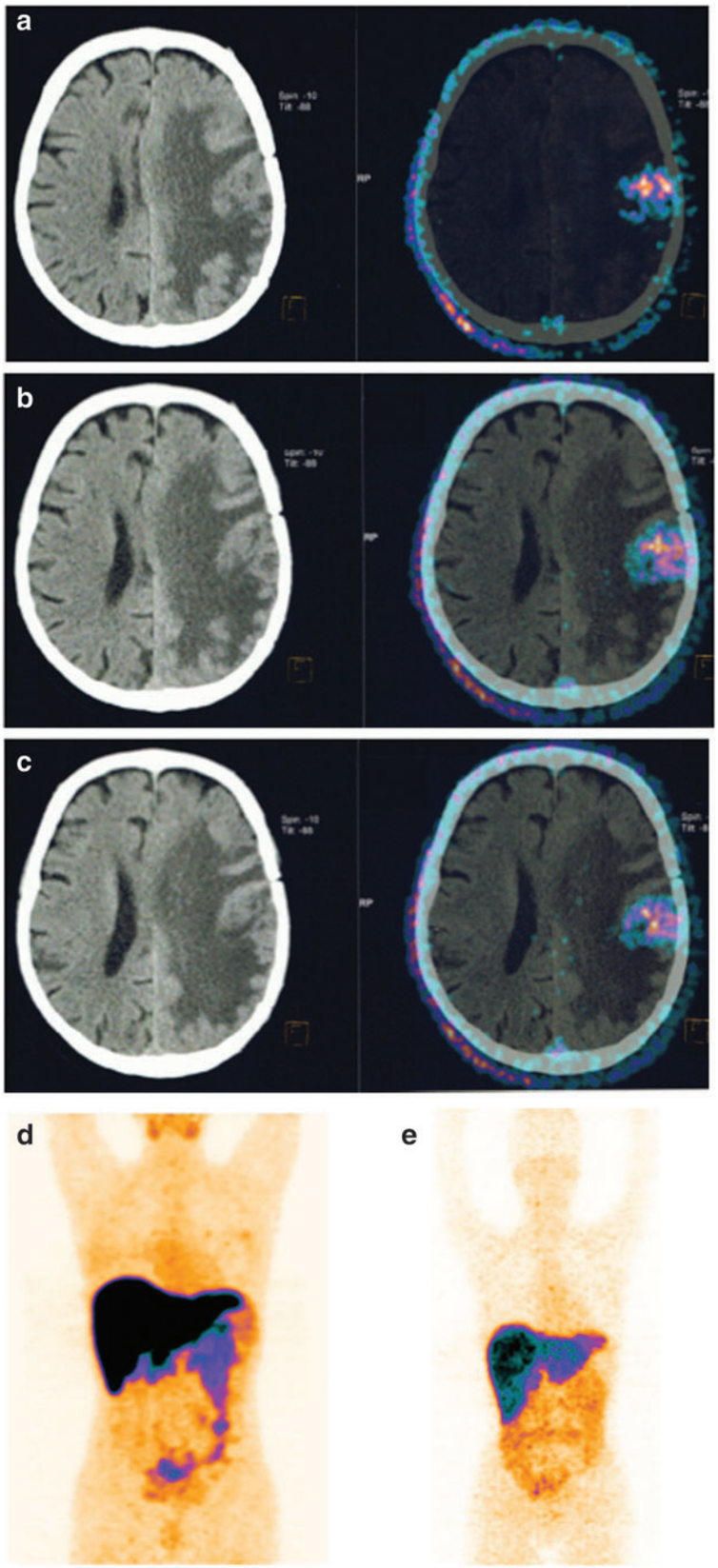

4C ▶

FIG. 2. CT (*left*) and PET/CT (*right*) brain images of patient 01 collected at **(a)** 1, **(b)** 3, and **(c)** 24 hours after injection of $^{64}CuCl_2$. Whole-body images of patient 05 collected at **(d)** 1 hour and **(e)** 24 hours after administration of the same tracer.

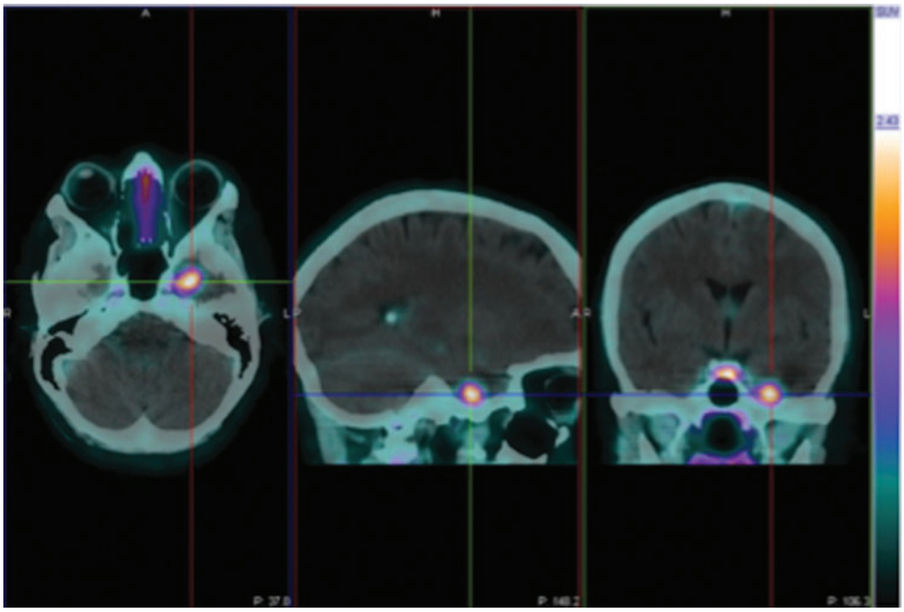

FIG. 3. PET/CT brain images of a patient with GBM associated to metastatic primary lung tumor (patient 016), collected at 1 hour after injection of $^{64}CuCl_2$ and showing cerebral lesions. ◀4C

diseases. Following this approach, an increasing number of investigations, in both animal models[32,33] and human subjects, are clearly showing that copper ions accumulate in various malignant tissues in a tumor-type dependent manner. For example, an early human study in prostate cancer patients has revealed that, after administration of $^{64}CuCl_2$, cancerous cells and metastatic lymph nodes selectively uptake radioactive copper ions, thus allowing a collection of diagnostic images of prostate tumor.[26] Along the same line, the present investigation was undertaken with the only purpose of obtaining first experimental evidence in human subjects that radioactive Cu-64 copper ions significantly accumulate in cerebral tumors and, therefore, could be potentially useful as a brain imaging agent. Since this work represents the first exploratory clinical study in humans where $^{64}CuCl_2$ was employed as a diagnostic tracer for cancers in the CNS, no comparison with previous studies of the same type was possible.

A limited number of patients (19) previously diagnosed with brain GBM were included in the study. Though a thorough comparison between MRI and Cu-64 PET imaging was not among the objectives of this study, MRI was selected as a standard diagnostic modality to assess the presence of brain cancerous lesions, which were further confirmed by biopsy. Figure 1 illustrates a representative example of results collected with MRI and PET/CT scans in one patient affected by GBM. Brain lesions were clearly visualized with both MRI and PET/CT imaging modalities with excellent congruity (Table 1). Analysis of SUV_{max} values at 1, 3, and 24 hours (Table 2) revealed a prolonged retention of activity into the brain tumor without significant washout after 24 hours. These values followed a ubiquitous trend toward increasing the concentration of radioactivity in the tumor at later times, a result that could be, presumably, ascribed to some delayed release of copper ions from the liver into the blood, which may function as an additional supply of the

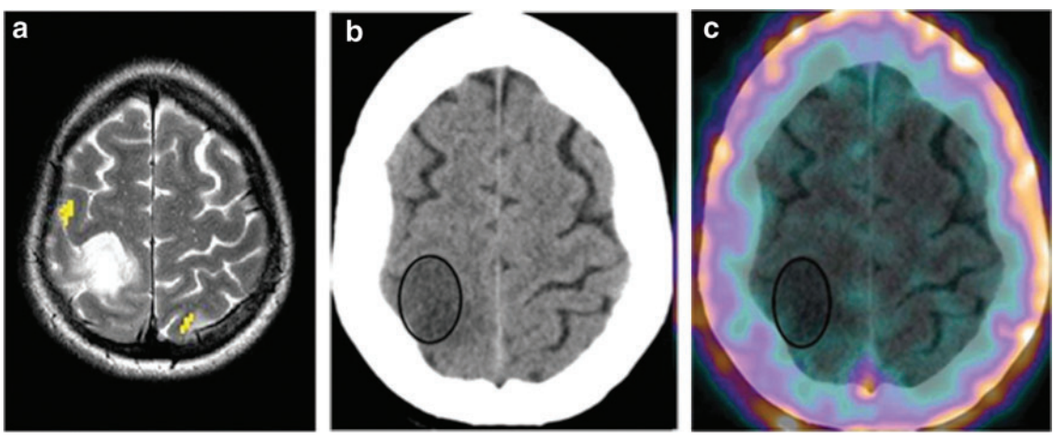

4C ▶

FIG. 4. MRI **(a)**, CT **(b),** and PET **(c)** images of a patient with grade II astrocytoma (patient 008) collected at 1 hour after injection of $^{64}CuCl_2$. No uptake was observed in the cerebral PET/CT scan.

Table 3. Organ-Normalized Cumulated Activity

Organ	*MBq hours/MBq*
Liver	6.90
Kidney	0.069
Red marrow	0.66
Spleen	0.027
Brain tumor	0.027
Total body	13.0

radiometal to tumor tissue, thus keeping almost stable the concentration of radioactivity into the cancerous lesions.

A consistent agreement between MRI and PET was also found in patients with brain lesions associated with a different primary cancer. It is interesting to note that visualization of cerebral metastases had been previously reported in a study on patients with neuroendocrine tumors injected with ^{64}Cu-DOTATATE.[34] This observation was tentatively attributed to uptake of the peptide radioconjugate by the metastatic tissue, although no reports of accumulation in CNS of DOTATATE derivatives radiolabeled with In-111, Ga-68, Tc-99m, Y-90, and Lu-177,[35,36] have been previously described. To solve this apparent conundrum and considering the results presented here, an alternative explanation would posit that radioactive copper ions were responsible for the observed brain localization. These ions could be arguably generated by some dissociation of the radioconjugate, and it is reasonable to expect that they will follow exactly the same biological pattern as described here for $^{64}CuCl_2$.

A sharp disagreement between MRI and PET/CT was found for the patient diagnosed with grade II astrocytoma (patient 008). MRI scan, undoubtedly, reveals the presence of the tumor in the left temporal lobe (Fig. 4, left). However, no uptake of $^{64}CuCl_2$ was detected in the same region as shown in Figure 4 (right). After surgical removal, histological characterization conclusively demonstrated no sign of active malignancy in this lesion. The lack of $^{64}CuCl_2$ accumulation in low-grade astrocytoma is somewhat surprising, since it may hint to some specific uptake mechanism of copper ions that seems active only in highly proliferating malignant cells.

Table 4. Estimates of Mean Absorbed Radiation Dose

Target organ	*Absorbed dose (mSv/MBq×10^{-2})*
Adrenals	2.91
Brain	3.42
Breasts	2.21
Gallbladder wall	4.63
Lower large intestine	4.53
Small intestine	4.98
Stomach wall	4.96
Upper large intestine	4.83
Heart wall	3.56
Kidneys	3.82
Liver	32.1
Lungs	2.96
Muscle	1.70
Pancreas	3.21
Red marrow	3.02
Osteogenic cells	3.98
Skin	2.12
Spleen	4.65
Testes	3.21
Thymus	2.35
Thyroid	1.95
Urinary bladder wall	2.30
Total body	3.12

Evidently, this conjecture requires more solid experimental evidence to be confirmed, but it prompts to consider some key problems related to the mechanism of uptake of Cu-64 ions in brain tumors. In particular, it raises the question of how positively charged copper ions were able to cross the blood–brain barrier (BBB) and diffuse into the cerebral region. Interestingly, preclinical studies in animals subcutaneously transplanted with U-87 MG cells revealed no brain localization of $^{64}CuCl_2$.[21] These findings give some support to the view that there might exist tumor-dependent uptake mechanisms for delivering $^{64}CuCl_2$ to cerebral tumors. An obvious assumption would be that Cu^{2+} ions are not freely circulating in the blood stream after injection, but they are presumably transported by some carrier protein. Although several proteins have been identified as copper carriers and transporters, including the high-affinity human copper transporter CTR1, which is also overexpressed in a variety of cancers,[16,17,37] it is hard at this time to provide a precise picture of the underlying biomolecular pathway. Similarly, it is hazardous to speculate whether copper ions are ferried through the BBB by some transport system, since in patients with brain tumors the permeability of the cerebral microvascular endothelium is usually altered, thus allowing the activation of tumor-specific exchange mechanisms[38–40] combined with some extravasation of ions and molecules into the nervous tissue.

Conclusions

This study reports the first evidence in humans that radioactive copper ions, when administered as chloride salt $^{64}CuCl_2$, are able to selectively accumulate in brain tumors and more specifically in GBM. No adverse events were observed after tracer injection, and prolonged retention of radioactivity was detected in cancerous lesions, followed by a slight increase of uptake at later times. This suggests that Cu-64 could be a potentially useful diagnostic agent for malignancies of the CNS. The conjecture that copper ions could be a specific marker of malignant cells was partially supported by the observation that no uptake of this radiometal was detected in a patient with low-grade astrocytoma. Although this observation was collected only in one patient and, therefore, requires stronger experimental evidence, it may suggest that the use of radioactive copper for imaging the *in vivo* behavior of the element copper, which has recognized multiple biological functions, might certainly open new routes to cancer detection and to a deeper biomolecular characterization of the cancerous lesion. However, to fully exploit this potential, extensive investigation of the biological pathway and the underlying mechanisms responsible for the passage of radioactive copper ions through BBB and subsequent accumulation in malignant brain tumors should be pursued. In addition, the clinical significance of findings described in this work remains to be established in larger, prospective studies.

Disclosure Statement

No competing financial interests exist.

References

1. Adamson DC, Rasheed BA, McLendon RE, et al. Central nervous system. Cancer Biomark 2010;9:193.
2. Kumthekar P, Raizer J, Singh S. Low-grade glioma. Cancer Treat Res 2015;163:75.
3. Cohen AL, Colman H. Glioma biology and molecular markers. Cancer Treat Res 2015;163:15.
4. Ostrom QT, Gittleman H, Stetson L, et al. Epidemiology of gliomas. Cancer Treat Res 2015;163:1.
5. Schiffer D, Valentini C, Melcarne A, et al. Spatial relationships of MR imaging and positron emission tomography with phenotype, genotype and tumor stem cell generation in glioblastoma multiforme, tumors of the central nervous system—Primary and secondary. In: Morgan LR (ed.). InTech, 2014, ISBN: 978-953-51-1576-2. Available from: www.intechopen.com/books/tumors-of-the-central-nervous-system-primary-and-secondary/spatial-relationships-of-mr-imaging-and-positron-emission-tomography-with-phenotype-genotype-and-tum AU5 ▶
6. Rosenkrantz AB, Friedman K, Chandarana H, et al. Current status of hybrid PET/MRI in oncologic imaging. AJR Am J Roentgenol 2016;206:162–172.
7. Puttick S, Bell C, Dowson N, et al. PET, MRI, and simultaneous PET/MRI in the development of diagnostic and therapeutic strategies for glioma. Drug Discov Today 2015;20:306.
8. Mabray MC,Barajas RF Jr, Cha S. Modern brain tumor imaging. Brain Tumor Res Treat 2015;3:8.
9. Chaumeil MM, Lupo JM, Ronen SM. Magnetic resonance (MR) metabolic imaging in glioma. Brain Pathol 2015; 25:769.
10. Schnell O, Krebs B, Carlsen J, et al. Imaging of integrin alpha(*v*)beta(3) expression in patients with malignant glioma by [^{18}F]galacto-RGD positron emission tomography. Neuro Oncol 2009;11:861.
11. Bell C, Dowson N, Fay M, et al. Hypoxia imaging in gliomas with ^{18}F-fluoromisonidazole PET: Toward clinical translation. Semin Nucl Med 2015;45:136.
12. Nedergaard MK, Michaelsen SR, Perryman L, et al. Comparison of ^{18}F-FET and ^{18}F-FLT small animal PET for the assessment of anti-VEGF treatment response in an orthotopic model of glioblastoma. Nucl Med Biol 2016;43:198.
13. Glaudemans AWJM, Enting RH, Heesters MAAM, et al. Value of ^{11}C-methionine PET in imaging brain tumours and metastases. Eur J Nucl Med Mol Imaging 2013;40:615.
14. Niccoli Asabella A, Cascini GL, Altini C, et al. The copper radioisotopes: A systematic review with special interest to ^{64}Cu. Biomed Res Int 2014;2014:786463.
15. Williams HA, Robinson S, Julyan P, et al. A comparison of PET imaging characteristics of various copper radioisotopes. Eur J Nucl Med Mol Imaging 2005;32:1473.
16. Kim BE, Nevitt T, Thiele DJ. Mechanisms for copper acquisition, distribution and regulation. Nat Chem Biol 2008; 4:176.
17. Lalioti V, Muruais G, Tsuchiya Y, et al. Molecular mechanisms of copper homeostasis. Front Biosci (Landmark Ed) 2009;14:4878.
18. Jørgensen JT, Persson M, Madsen J, et al. High tumor uptake of (64)Cu: Implications for molecular imaging of tumor characteristics with copper-based PET tracers. Nucl Med Biol 2013;40:345.
19. Brady DC, Crowe MS, Turski ML, et al. Copper is required for oncogenic BRAF signalling and tumorigenesis. Nature 2014;509:492.
20. Ishida S, Andreux P, Poitry-Yamate C, et al. Bioavailable copper modulates oxidative phosphorylation and growth of tumors. PNAS 2013;110:19507.
21. Ferrari C, Asabella AC, Villano C, et al. Copper-64 dichloride as theranostic agent for glioblastoma multiforme: A preclinical study. BioMed Res Int 2015; 2015. DOI:10.1155.2015.129764
22. McCarthy DW, Shefer RE, Klinkowstein RE, et al. The efficient production of high specific activity Cu-64 using a biomedical cyclotron. Nucl Med Biol 1997;24:35.
23. Jones-Wilson TM, Deal KA, Anderson CJ, et al. The in vivo behavior of copper-64-labeled azamacrocyclic complexes. Nucl Med Biol 1998;25:523.
24. Kinahan PE, Fletcher JW. PET/CT standardized uptake values (SUVs) in clinical practice and assessing response to therapy. Semin Ultrasound CT MR 2010;31:496.
25. Stabin MG, Sparks RB, Crowe E. Olinda/EXM: The second generation personal computer software for internal dose assessment in nuclear medicine. J Nucl Med 2005; 46:1023.
26. Capasso E, Durzu S, Piras S, et al. Role of $^{64}CuCl^2$ PET/CT in staging of prostate cancer. Ann Nucl Med 2015;29:482.
27. Duatti A. Molecular imaging with endogenous and exogenous ligands: The instance of antibodies, peptides, iodide and cupric ions. Nucl Med Biol 2015;42:215.
28. Qin C, Liu H, Chen K, et al. Theranostics of malignant melanoma with $^{64}CuCl_2$. 2014;55:812.
29. Peng F. Positron emission tomography for measurement of copper fluxes in live organisms. Ann N Y Acad Sci 2014; 1314:24.
30. Scheiber IF, Mercer JF, Dringen R. Metabolism and functions of copper in brain. Prog Neurobiol 2014;116:33.
31. Hueting R. Radiocopper for the imaging of copper metabolism. J Labelled Comp Radiopharm 2014;57:231.
32. Peng F, Lu X, Janisse J, et al. PET of human prostate cancer xenografts in mice with increased uptake of $^{6}4CuCl_2$. J Nucl Med 2006;47:1649.
33. Zhang H, Cai H, Lu X, et al. Positron emission tomography of human hepatocellular carcinoma xenografts in mice using copper (II)-64 chloride as a tracer with copper (II)-64 chloride. Acad Radiol 2011;18:1561.
34. Pfeifer A, Knigge U, Mortensen J, et al. Clinical PET of neuroendocrine tumors using ^{64}Cu-DOTATATE: First-in-humans study. J Nucl Med 2012;53:1207.
35. Johnbeck CB, Knigge U, Kjær A. PET tracers for somatostatin receptor imaging of neuroendocrine tumors: Current status and review of the literature. Future Oncol 2014;10:2259.
36. Kjaer A, Knigge U. Use of radioactive substances in diagnosis and treatment of neuroendocrine tumors. Scand J Gastroenterol 2015;50:740.
37. Holzer AK, Varki NM, Le QT, et al. Expression of the human copper influx transporter 1 in normal and malignant human tissues. J Histochem Cytochem 2006;54:1041.
38. Avsenik J, Bisdas S, Popovic KS. Blood-brain barrier permeability imaging using perfusion computed tomography. Radiol Oncol 2015;49:107.
39. Heye AK, Culling RD, Valdés Hernández Mdel C, et al. Assessment of blood-brain barrier disruption using dynamic contrast-enhanced MRI. A systematic review. Neuroimage Clin 2014;6:262.
40. Dubois LG, Campanati L, Cassia Righy C, et al. Gliomas and the vascular fragility of the blood brain barrier. Front Cell Neurosci 2014;8:1.

AUTHOR QUERY FOR CBR-2016-2028-VER9-PANICHELLI_1P

AU1: Please note that gene symbols in any article should be formatted as per the gene nomenclature. Thus, please make sure that gene symbols, if any in this article, are italicized.
AU2: Please review all authors' surnames for accurate indexing citations.
AU3: Please confirm the address of correspondence.
AU4: The Publisher requests for readability that no paragraph exceeds 15 typeset lines. Please check for long paragraphs and divide where needed.
AU5: Please provide the date of access for Ref. 5.